Pergamon

PII: S0191–8141(98)00026–1

Journal of Structural Geology, Vol. 20, No. 7, pp. 917 to 935, 1998

0191-8141/98 $19.00 + 0.00

Grain boundary hierarchy development in a quartz mylonite

PATRICK W. TRIMBY, DAVID J. PRIOR and JOHN WHEELER

Department of Earth Sciences, University of Liverpool, L69 3BX, U.K., E-mail: patster@liv.ac.uk

(*Received* 12 *June* 1997; *accepted in revised form* 2 *March* 1998)

Abstract—Orientation contrast imaging using forescatter detectors and backscattered electron diffraction techniques in the scanning electron microscope have been used to investigate the boundary hierarchy characteristics of a quartz mylonite shear zone from Torridon, NW Scotland. The boundary hierarchy is defined as the relationship between the boundary misorientations, their enclosed domain size and their frequency distribution. By measuring the misorientation across every grain and subgrain boundary, the characteristics of the boundary hierarchy can be found. Two microstructural domains were studied: one partially recrystallized low strain domain with large relict grains and one fully recrystallized high strain mylonitic domain. Our results indicate that the processes of recovery, subgrain rotation and grain boundary migration recrystallization each produce identifiable boundary hierarchy signatures. In the relict quartz grains we have identified the processes of recovery and subgrain rotation; in the recrystallized quartz a cyclic steady state exists between these and other processes. Coupling these data with traditional microstructural observations allows a more rigorous investigation into the development of a high strain, fine grained mylonite from a coarse grained, undeformed protolith. We suggest that this type of detailed crystallographic microstructural analysis can greatly further our understanding of microstructural development in shear zones and may have implications for the effective use of (sub)grain size palaeopiezometers.

INTRODUCTION

The nature and behaviour of boundaries within and between grains undoubtedly has a significant effect on the rheological and petrophysical properties of rocks (e.g. White and White, 1981; McLaren, 1986; Fliervoet, 1995; Lloyd *et al*., 1997). However, the use of boundaries to characterize and quantify microstructures is a time consuming and problematical procedure. To describe comprehensively a boundary, five degrees of freedom need to be considered (e.g. McLaren, 1986; Lloyd *et al*., 1997): one to specify the magnitude of the angular misorientation, θ, between the two crystal lattices; two to define the axis of this rotation and two to define the orientation of the actual boundary relative to one of the grains. Due to the practical difficulties of determining the actual boundary orientation (e.g. using serial sectioning), most grain boundary studies concentrate on the misorientation rotation axis and magnitude. However, such studies are presently only able to relate the boundary misorientation rotation axis and magnitude to the spatial characteristics of a relatively small number of grains (e.g. Fliervoet and White, 1995; Lloyd and Freeman, 1991, 1994; Lloyd *et al*., 1997). This paper introduces a technique which, using only the misorientation magnitude, θ, characterizes microstructures consisting of substantial numbers of grains. Although this utilizes only one of the five aforementioned degrees of freedom, we show that this does not constitute an unjustified simplification of grain boundaries, and we compare our results with data collected in the manner of earlier studies.

Backscattered electron (BSE) diffraction in the scanning electron microscope (SEM) allows the easy identification of the crystallographic orientation of any particular grain or subgrain in geological specimens (Lloyd *et al*., 1987; Dingley and Randle, 1992; Lloyd, 1995). This in turn can give the angular magnitude and rotation axis of misorientation across any particular grain or subgrain boundary. The spatial distribution of boundary misorientation magnitudes within a ductile shear zone will relate to any boundary hierarchy present. Thus the grain boundary hierarchy is defined as the relationship between boundary misorientations and the size of domains they enclose, as well as the frequency distribution of boundary misorientations. This paper presents boundary hierarchy data from quartz mylonites in a shear zone and relates the boundary hierarchy characteristics to the observed microstructures. We also illustrate that the hierarchy information is, in its own right, a useful tool in helping to identify the processes of recovery and recrystallization in operation during the shear zone's microstructural evolution.

Ductile shear zones allow us to study the development of a mylonitic microstructure with increasing strain (White *et al*., 1980; Law *et al*., 1990; Lloyd *et al*., 1992). A margin to interior transect in a ductile shear zone can be interpreted as a temporal section, but this holds true only if the shear zone did not widen with time (Means, 1995). The processes of dynamic recovery and recrystallization have been well documented and are generally accepted to occur simultaneously during deformation (e.g. White, 1977). However, the relative importance of the individual processes of recovery, subgrain rotation and grain

boundary migration is harder to establish. As will become clear, the terminology applied to boundaries and processes associated with boundaries can be misleading. The terminology we shall use is defined in Table 1 and is explained over the following paragraphs.

The effect of straining a crystal lattice is to increase the density of dislocations within that lattice, commonly with an excess of dislocations of one sign (Cottrell, 1964); the driving force for both recovery and recrystallization is the rearrangement and elimination of these dislocations and the subsequent lowering of the intracrystalline strain energy. Recovery is the process by which the dislocations of one predominant sign glide and climb (climb being the rate limiting process) to form subgrain walls in order to localize these defects and reduce the overall plastic strain energy; this results in a return to the original physical properties of the undeformed crystal of domains bounded by subgrain walls. Non-geometrically necessary dislocations are annihilated causing the geometrically necessary dislocations to predominate (White, 1977). The microstructural signature is one of evenly spaced subgrain walls, commonly forming a distinctive polygonal outline with many subgrain boundaries intersecting at 90° (Hobbs *et al.*, 1976). The continued movement of dislocations into an existing subgrain wall, with climb as the rate controlling step, will increase the misorientation across the subgrain wall if the discrete dislocations have the same sign as the wall. This process is often called subgrain rotation although it is indistinguishable from the process of recovery. In this paper we shall use the term recovery to mean the formation of a new subgrain wall and the term subgrain rotation to mean the increase of misorientation across a subgrain wall due to the continued movement of dislocations into that wall.

Recrystallization is the process by which internal strain energy is reduced by the formation and develop-

Table 1. A summary and explanation of the terms used in this paper

	Boundaries
	Refer only to boundaries between like phases
Subgrain wall	A planar or curviplanar array of dislocations where the dislocation cores do not overlap.
Grain boundary	A planar or curviplanar boundary, where the structure of the boundary is not simply related to the structure of grains on either side.
Optical subgrain wall	A boundary which has low optical relief and a small change in extinction angle across it.
Optical grain boundary	A boundary which has high optical relief and a large change in extinction angle across it.
min θ Domain boundary	A boundary across which there is a crystallographic mismatch equal to or greater than θ.
	Domains
Subgrain	Domain enclosed by boundaries, where at least part of the boundary is a subgrain wall.
Grain	Domain enclosed entirely by grain boundaries.
Optical subgrain	Domain enclosed by boundaries, where at least part of the boundary is an optical subgrain wall.
Optical grain	Domain enclosed entirely by optical grain boundaries.
min θ Domain	Domain enclosed by boundaries, where the minimum misorientation across any part of the boundary is θ.
	Processes
Recovery	The generation of a subgrain wall through glide and climb.
Subgrain rotation	The increase of misorientation across an existing subgrain wall by addition of further dislocations by glide or climb.
Subgrain rotation recrystallization	The addition of a dislocation to a subgrain wall so that the dislocation cores in the boundary overlap and the boundary must be redefined as a grain boundary.
Grain boundary migration recrystallization	Strain induced migration of a grain boundary by detachment of atoms from one grain and diffusion into the grain boundary structure, simultaneous with diffusion of atoms out of the grain boundary structure and into the other grain.
Grain boundary sliding	Relative movements of grains along the plane of the grain boundary.
Nucleation	Generation of a new grain, smaller than existing grains.

ment of new grains. There are two commonly quoted recrystallization mechanisms:

Subgrain rotation recrystallization

If subgrain rotation, as defined above, continues, then a stage may be reached where addition of an extra dislocation to a subgrain wall will mean that it can no longer be described simply in terms of lattice dislocations because of the overlap of dislocation cores (Drury and Urai, 1990). Such a boundary will have a structure independent of the domains on either side of it and is commonly known as a grain boundary. The change from a subgrain wall to a grain boundary will alter the properties of that boundary and may be thought of as a recrystallization process. This process is commonly referred to as subgrain rotation recrystallization (Guillopé and Poirier, 1979). A core and mantle microstructure, as described by White (1976) and Lloyd and Freeman (1994) is typical of subgrain rotation recrystallization.

Strain induced grain boundary migration

Synkinematic microscopy during deformation of transparent polycrystals (Urai *et al.*, 1986; Means, 1989) shows, quite spectacularly, that boundaries between grains migrate through the crystalline material. Migration occurs by a diffusional process—material is detached from the lattice on one side of the boundary, diffused across the boundary and attached to the lattice on the other side. The process is driven by differential intracrystalline strain energy—grains with low defect densities consume grains with higher defect densities. A subgrain wall would be unlikely to maintain its identity as a simple array of dislocations during a migration process accommodated by across-boundary diffusion. However, it is understood that subgrain walls can move by synchronous glide/climb of the dislocations in the wall (Urai *et al.*, 1986) but this process is a subgrain rotation process and is distinct from grain boundary migration. Sutured grain boundaries are recognized as being characteristic of grain boundary migration recrystallization (e.g. Urai *et al.*, 1986).

It is clear from the discussion in the preceding paragraphs that the distinction of subgrain walls and grain boundaries is an important one. Similarly important is the distinction of subgrains, where part of the enclosing boundary is a subgrain wall, from grains, where all of the enclosing boundary is a grain boundary. Objective assessment of whether a boundary is a subgrain wall or a grain boundary can only be unequivocally made using transmission electron microscopy (TEM). The subgrain rotation recrystallization model predicts that there should be a relationship between the nature of a boundary and the misorientation across it. There are few comprehensive TEM studies of geologically important minerals to show the relationship of misorientation and the nature of the boundary. However, one such study, Fitzgerald *et al.* (1983), shows that there is a change in the boundary characteristics in albite at very low misorientations (1–5°). McLaren (1986) shows that the relationships of misorientation and boundary characteristics in quartz are rather more complex.

Without detailed TEM studies the nature of a boundary can only be constrained from the nature of the misorientation across it. In many studies an arbitrary misorientation value is assigned, above which boundaries are assumed to be grain boundaries and below which they are assumed to be subgrain walls although, in some cases (e.g. quartz), this value corresponds to the necessary misorientation for the overlap of dislocation cores. Typical values are 10° for quartz (White, 1977), 15° or more for halite (Guillopé and Poirier, 1979) and 15° for olivine (Poirier and Nicolas, 1975). In transmission optical microscopy this approach is particularly appealing as higher angle boundaries show higher relief and low angle boundaries can be identified by small

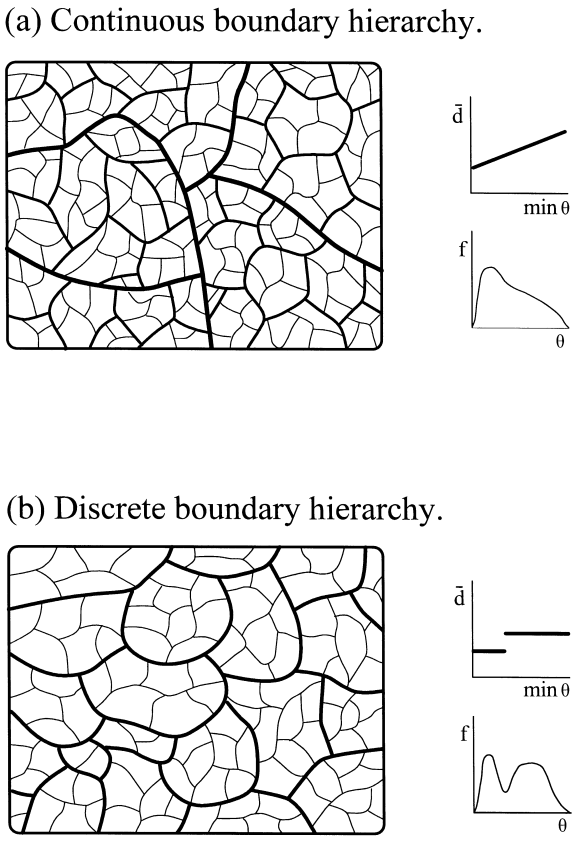

Fig. 1. Schematic illustration of two theoretical boundary hierarchies and their associated domain size and boundary misorientation distribution characteristics. (a) 'Continuous' boundary hierarchy, showing a schematic microstructure with line thickness proportional to boundary misorientation. The expected mean enclosed domain size ($\bar{d}$) against minimum misorientation of enclosing boundaries (min θ) and frequency (f) against misorientation (θ) graphs are plotted. (b) 'Discrete' boundary hierarchy, showing a schematic microstructure, and the expected $\bar{d}$ vs min θ and f vs θ graphs. See text for discussion.

changes in extinction position. In this study grain boundaries, grains, subgrain walls and subgrains identified using these commonly applied criteria will be preceded by the word optical.

Orientation contrast images in the SEM (Lloyd, 1987; Prior *et al.*, 1996) display the boundaries between domains of similar crystallographic orientation but neither the nature of the domain boundaries nor the misorientation across them can be assessed from the image. Backscattered electron diffraction techniques such as electron channelling (Lloyd, 1987) and electron backscatter diffraction (EBSD: Venables and Harland, 1972; Dingley, 1984; Dingley and Randle, 1992) enable precise measurement of domain orientations and thus the misorientations across domain boundaries.

In any tectonite there is a range of boundary misorientation values and there will exist some sort of boundary hierarchy. Intuitively the low angle boundaries will enclose a smaller domain size than the higher angle boundaries. It is possible to envisage a continuous hierarchy in which progressively larger misorientations enclose progressively larger domain sizes (Fig. 1a); the frequency of boundaries with specific misorientations will decrease with increasing θ (Fig. 1a). A second possibility is a 'discrete' hierarchy in which there are steps in the domain size defined by progressively larger misorientations (Fig. 1b). This could possibly result in a bimodal frequency distribution of boundary misorientations, due to an abundance of both very low and high misorientation boundaries (Fig. 1b).

In this contribution we use the microstructures in a sheared quartz vein to investigate the variations in grain boundary hierarchies with increasing shear strain. We shall present the results from a detailed crystallographic analysis and show how some hierarchy characteristics may be attributed to particular recrystallization histories. Finally we shall discuss some of the implications, uses and future developments of this technique.

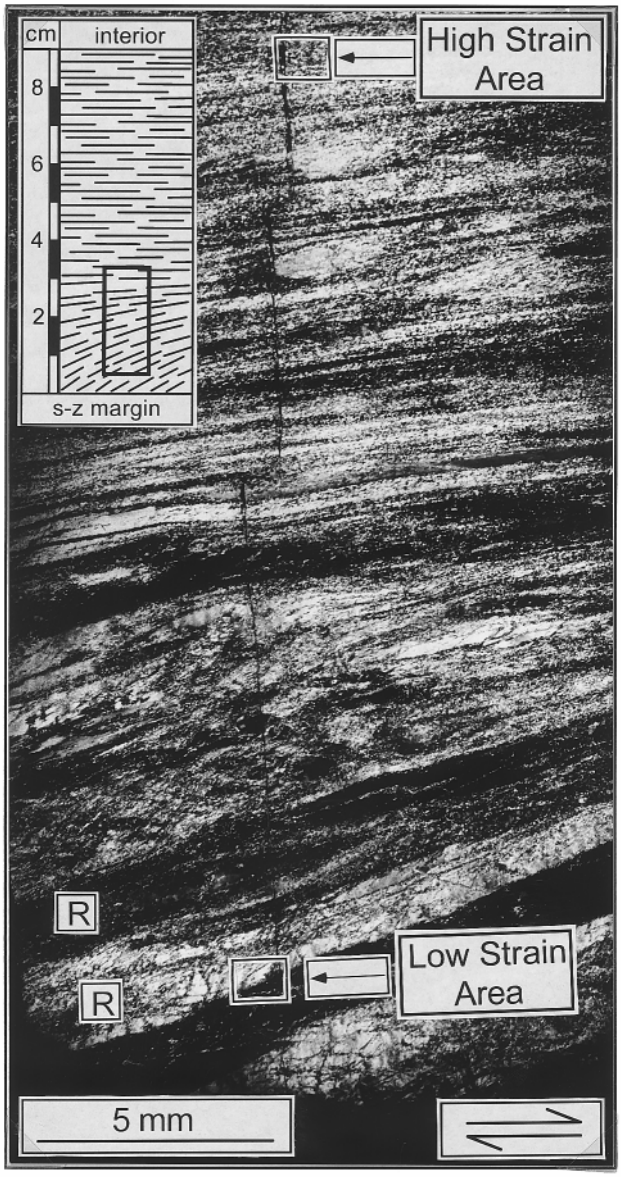

Fig. 2. Photomicrograph of the shear zone margin, taken under crossed polarized light. Large relict grains (R) are clearly visible, separated by narrow bands of fine grained matrix quartz. The homogeneous microstructure of the high strain interior can be seen at the top of the photomicrograph. The studied areas are marked. The inset shows the position of the photomicrograph relative to the whole sample.

SAMPLE AND ANALYTICAL DETAILS

Sample location

The sample studied came from a deformed planar quartz vein lying along a joint within the Lewisian basement gneiss in Torridon, NW Scotland. The vein is approximately 20 cm thick and can be traced across the outcrop for 40 m; it shows a very strong mineral stretching lineation on surfaces parallel to the vein walls. The surrounding gneiss shows no deformation associated with the vein: it is assumed that the gneiss acted as a rigid body throughout the deformation of the vein. The characteristics of this shear zone are extremely similar to that studied by Law *et al.* (1990), sampled 700 m to the south.

Sample description

The sample is almost 100% quartz, with a few feldspar porphyroclasts up to 2 mm in diameter. A section through the vein was cut parallel to the lineation and perpendicular to the foliation (the XZ section of the strain ellipsoid, with $X \geqslant Y \geqslant Z$). The work presented in this contribution concentrates on a single surface cut in this orientation and made into polished thin sections for observation with both an optical microscope

and a SEM. The section shows a considerable variation in strain from the margin to the interior (Fig. 2); we have assumed the margin is indicative of zero strain. The mylonitic foliation within this vein shows the orientation variation expected for heterogeneous simple shear deformation (Ramsay and Graham, 1970; Law *et al.*, 1990); the foliation is orientated at $\approx 44^\circ$ to the vein walls at the shear zone margin and bends around to a minimum angle of $\approx 3^\circ$ to the vein walls in the shear zone interior.

Studies of a relatively undeformed quartz vein sampled 40 m to the west show microstructures with regular optical grain sizes of approximately 10 mm, with no particular crystallographic fabric, little optical subgrain structure and just a few discrete low angle boundaries. This we have taken to be similar to the undeformed protolith of the studied vein.

The variation in microstructure from the margin to the interior in the deformed vein is complex as seen in Fig. 2. Large ribbon quartz features define a fabric that bends into a plane sub-parallel to the shear zone margin accompanied by a significant reduction in optical grain size. There is no apparent change in the microstructure from a distance of 25 mm from the shear zone margin to the shear zone interior. The microstructure can be divided into two distinct zones: the low strain margin zone and the high strain interior zone. The low strain margin zone is characterized by the presence of the aforementioned large, elongate quartz grains inferred to be a remnant feature of the original vein microstructure; these we have called 'relict' grains (Fig. 2). The high strain interior zone has a more homogeneous microstructure, consisting entirely of fine ($< 20\ \mu$m) optical grains of quartz (Fig. 2). The transition between the two zones is gradual, with an increase in the proportion of fine grained quartz with increasing strain.

Analytical procedures

Imaging techniques. Thin sections, 30 μm thick, were polished to 0.25 μm using diamond paste on a paper lap and then using SYTON fluid on a polyurethane lap to remove all remaining surface damage (Lloyd, 1987). The sections were coated with an extremely thin carbon coat to reduce charging effects during SEM work. The microstructures were then imaged using a standard polarizing optical microscope under crossed polarized light. The same area was then imaged in the SEM using forescatter detectors (Prior *et al.*, 1996). Forescatter detectors provide a high resolution orientation contrast (OC) image comparable to those obtained using electron channelling (Lloyd, 1987). However, the detector geometry allows the synchronous use of electron backscatter diffraction (EBSD) techniques for the collection of absolute crystallographic orientation data. The forescatter image is purely qualitative so that very low angle misorientations can appear as high contrast changes in the final image while some high angle boundaries may be invisible due to crystal lattice and geometrical coincidences. Several images taken at slightly different electron beam–specimen configurations are required in order to see *all* the domain boundaries (Prior *et al.*, 1996). All the forescatter images were taken using the same magnification to prevent the introduction of artificial domain size changes due to scale alterations. The SEM was operated with an accelerating voltage of 20 kV, a working distance of 24–28 mm and with a beam current of ≈ 0.8 nA.

Crystallographic techniques. For this study, electron backscatter patterns (Alam *et al.*, 1954; Venables and Harland, 1972; Dingley, 1984; Dingley and Randle, 1992) were collected from individual domains using the SEM, operating with a greater beam current (10–15 nA). Each electron backscatter pattern (EBSP) was indexed automatically using the software CHANNEL+ (Schmidt and Olesen, 1989) using a reference file of 99 *hkl* planes within the quartz structure. This enabled the determination of the absolute crystallographic orientation of any individual domain to be determined. The spatial resolution of this technique is $\approx 1\ \mu$m whilst the angular resolution is 1–2° relative to the specimen axes (i.e. the x, y and z directions) but 0.5–1° relative to other measurements within the same specimen. This allows the misorientation across any individual domain boundary to be determined to within 1° accuracy. In calculating misorientations, the trigonal symmetry of quartz results in six equivalent misorientation axes and magnitudes. It is convention to take the misorientation with the minimum magnitude, although this may not be the absolute answer (e.g. Randle and Ralph, 1986; Randle, 1992; Fliervoet and White, 1995).

Analysis of data. Two separate areas were analysed in this study (Fig. 2): one from within the low strain margin zone, 10 mm from the shear zone margin, and one from within the high strain interior zone, 30 mm from the shear zone margin. Once each area had been imaged, both optically and using the SEM, and EBSPs had been collected and indexed, the following steps were followed:

1. The minimum angular misorientation across every domain boundary was calculated and plotted as the 'correlated boundary misorientation distribution' histogram. This is a frequency against misorientation plot of misorientations between neighbouring domains (Fliervoet *et al.*, 1997).
2. Domain boundary misorientation maps were produced. For instance, a map showing all the boundaries with an angular misorientation of 10° or greater is a $\geq 10^\circ$ boundary misorientation map. This in turn defines a specific domain size for a

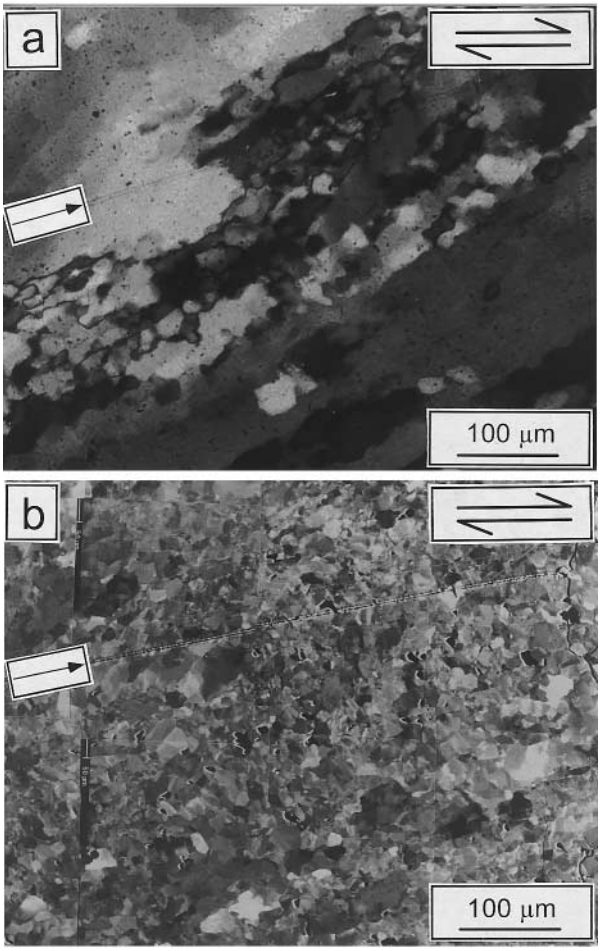

Fig. 3. The low strain margin zone. (a) Photomicrograph taken under crossed polarized light. (b) Forescatter image of the same area taken using the SEM. Operating conditions: Acc.V. 20 kV; WD 26 mm. Arrow marks position of a polishing scratch on both images.

$\geq 10^\circ$ misorientation. The same process was carried out for boundaries with misorientations $\geq 8^\circ$, $\geq 6^\circ$, $\geq 4^\circ$ and $\geq 2^\circ$. Where the misorientation was below 2° yet a visible shift in the EBSP occurred from one domain to the other, the misorientation must be between the minimum visible in an OC image, estimated at 0.1° (Prior *et al.*, 1990) and 3° ($2 \pm 1^\circ$). These boundaries have been assigned a misorientation of 1° and have been used to draw a $\geq 1^\circ$ misorientation map.

3. Domain sizes in each misorientation map were analysed using NIH Image 1.61, using the mean diameter of each domain as a measure of its size. The mean diameter was taken as the average of the long and short axes of a best fit ellipse.
4. For each misorientation map (from $\geq 1^\circ$ to $\geq 10^\circ$) the mean domain size ($\bar{d}$) defined by a particular misorientation map was plotted against the minimum misorientation (min θ) to show the characteristics of the boundary hierarchy.

RESULTS

Low strain margin zone

Microstructure. The microstructure of the low strain area is illustrated in the optical and forescatter images in Fig. 3. Parts of large, relict grains are clearly visible, separated by narrow bands of fine grained 'matrix' quartz. The two images show markedly different features of the overall microstructure: the optical image clearly shows the large relict grains that characterize this low strain zone and these show undulose extinction. The fine grained matrix bands are visible in between the relict grains and, in places, forming narrow zones cutting across or wholly within relict grains. In places straight, evenly spaced optical subgrain boundaries typical of recovery can be seen within these grains. The size of the matrix optical grains is too small ($< 25\ \mu$m) to allow any detailed examination of their substructure using optical microscopy with 30 μm thin sections.

The forescatter image is qualitative (i.e. no correlation between the grey-scale and orientation) with the result that the final image shows little of the overall relict microstructure. However, the superior resolution and sensitivity to crystallographic orientation differences allow a detailed inspection of the substructure both in the relict grains and in the matrix domains. The two microstructural regions identified with the polarizing microscope can be distinguished, albeit subtly, in the forescatter image by a number of noticeably larger domains within the relict grains. The domains within the relict grains also appear to have a more strain free interior than those in the fine grained matrix, with little evidence of irregular variations in OC.

Crystallographic preferred orientation. Figure 4 shows pole figures taken from both the relict grains and the matrix in this zone. The *c*-axis pole figures show the tight clustering expected for the relict grains and clearly three distinct relict grains can be identified. These three distinct orientations are also visible in the optical photomicrograph (Fig. 3a). The matrix domain *c*-axes and *a*-axes also show clustering around the same orientations as the three relict grains, however, a number of the domains have orientations with no apparent link with the relict grain orientations.

Domain boundary hierarchies. The EBSD technique was used to analyse 738 domains, and the misorientations across 1912 domain boundaries were calculated. Boundary misorientation maps for $\geq 1^\circ$, $\geq 2^\circ$, $\geq 4^\circ$, $\geq 6^\circ$, $\geq 8^\circ$ and $\geq 10^\circ$ boundary misorientations were produced and, from these, the defined domain sizes were measured. Figure 5 shows two of these misorientation maps, for $\geq 4^\circ$ and $\geq 10^\circ$ boundary misorientations. The relict grain microstructure is clearly visible in both, especially in the $\geq 10^\circ$ misorientation map. The domain size data, measured directly from the misorien-

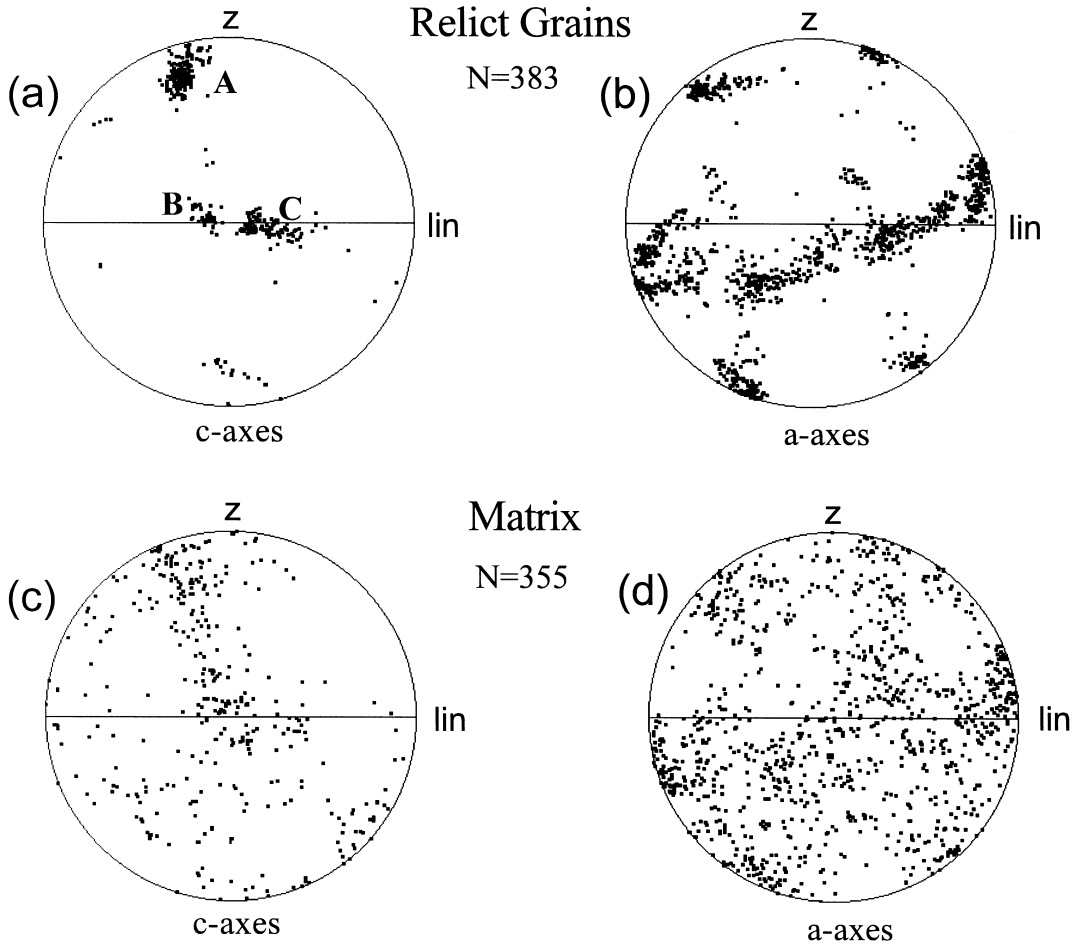

Fig. 4. Pole figures from the low strain zone. (a) *c*-axes from the relict grains. A, B and C mark tight clusters indicative of three relict grain orientations. (b) *a*-axes from the relict grains. (c) *c*-axes from the matrix domains. (d) *a*-axes from the matrix domains.

tation maps, are plotted in Fig. 6(a). The data from the two microstructural regions have been plotted separately (Fig. 6b). For the matrix domains, the size distribution is approximately log-normal; the lower number of relict domains makes statistical characterization more difficult.

The matrix region shows a discrete boundary hierarchy, with a single step between min $\theta = 1^\circ$ and min $\theta = 2^\circ$ where the domain size jumps from $\bar{d} = 12\ \mu$m to $\bar{d} = 18\ \mu$m. The domain size increases very little from min $\theta = 2^\circ$ ($\bar{d} = 18\ \mu$m) to min $\theta = 10^\circ$ ($\bar{d} = 19\ \mu$m), indicating a relative absence of domain boundaries within this misorientation range. The microstructure is defined by a large domain size ($\bar{d} = 18$–$19\ \mu$m) composed dominantly of $\geq 10^\circ$ boundaries. Within these domains are some $< 2^\circ$ boundaries which define a smaller domain size ($\bar{d} = 12\ \mu$m).

The relict grains show a more continuous boundary hierarchy with an increase in domain size from $\bar{d} = 13\ \mu$m for min $\theta = 1^\circ$ to $\bar{d} = 57\ \mu$m for min $\theta = 10^\circ$ in similar sized steps. These data indicate that domains defined by $\geq 10^\circ$ boundaries contain $\geq 8^\circ$ boundaries which define a smaller domain size. These in turn contain $\geq 6^\circ$ boundaries which define an even smaller domain size. This continues down to the smallest misorientations which define a relatively small domain size ($\bar{d} = 13\ \mu$m). Note that the min $\theta = 1^\circ$ domain size for both the relict grains and the matrix is approximately equal.

The approach followed in Fig. 6(a) is analogous to the definition of optical grain size and optical subgrain size, although it is much more objective and rigorous. However, the shape of the graph in Fig. 6 is dependent not only on the boundary hierarchy characteristics but also on the boundary topology and the frequency of particular boundary misorientations. The data have also been plotted as frequency histograms for the boundary misorientations. Figure 7 shows the boundary misorientation distribution for the relict grains (Fig. 7a) and the matrix (Fig. 7b). The relict grains contain a large number of very low angle ($< 2^\circ$) boundaries, with the frequency decreasing exponentially with increasing misorientation. There are very few boundaries with misorientations $> 12^\circ$ within the relict grains. The matrix also has a high number of very low angle boundaries, but fewer in the 2–10°

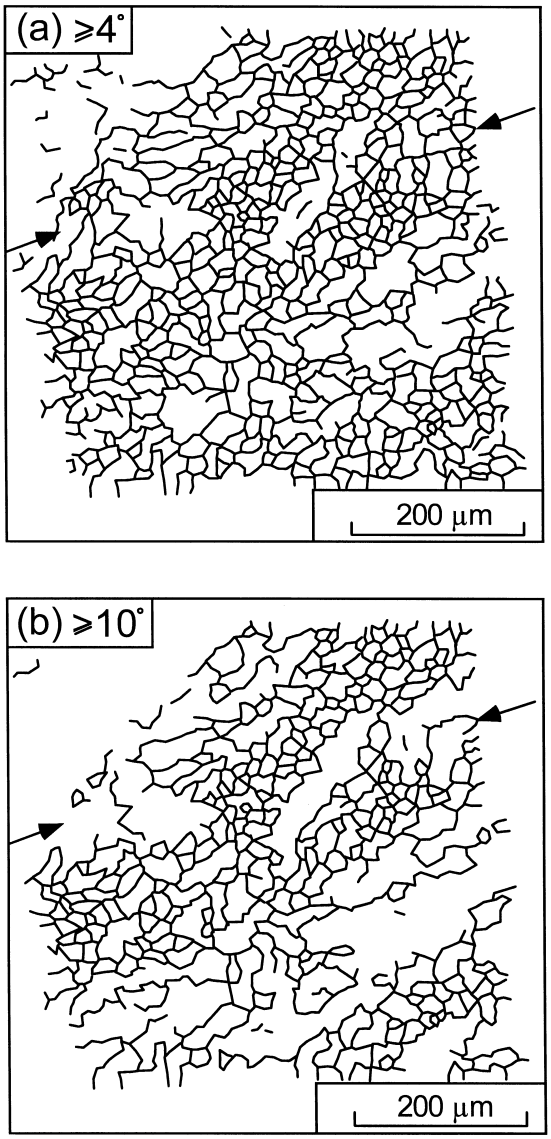

Fig. 5. Boundary misorientation maps for the low strain zone. (a) Boundaries with ≥4° misorientation. (b) Boundaries with ≥10° misorientation. Arrows mark the position of the polishing scratch visible in Fig. 3.

range. There is a small peak at 80–90°, and a larger peak at 55–60°. This 55–60° peak is due to a significant number of Dauphiné twin boundaries (60° rotation about the *c*-axis). A detailed analysis of the misorientation axes of these boundaries shows that approximately 40% of those matrix boundaries with 55–60° misorientations have a rotation axis within 15° of the *c*-axis. For the relict grain boundaries this figure is nearer to 80%.

High strain interior zone

Microstructure. The microstructure of the high strain zone is illustrated in the optical and forescatter images in Fig. 8. The two images are very similar, although the forescatter image does show greater detail of the microstructure within optical grains. Optical grains show a preferred elongation at a small angle to the shear zone margin, as observed in similar quartz shear zones (e.g. Law *et al*., 1990; Lloyd *et al*., 1992); their size is approximately constant throughout the high strain interior zone and, at $< 20\ \mu$m, is too small to be accurately analysed using optical microscopy with 30 μm thin sections. The forescatter image also shows some preferred elongation in the same direction, but the domains are considerably smaller than the optical grains.

Crystallographic preferred orientation. Figure 9 shows the pole figures for the high strain interior zone. The *c*-axes define part of a strong girdle with a maxi-

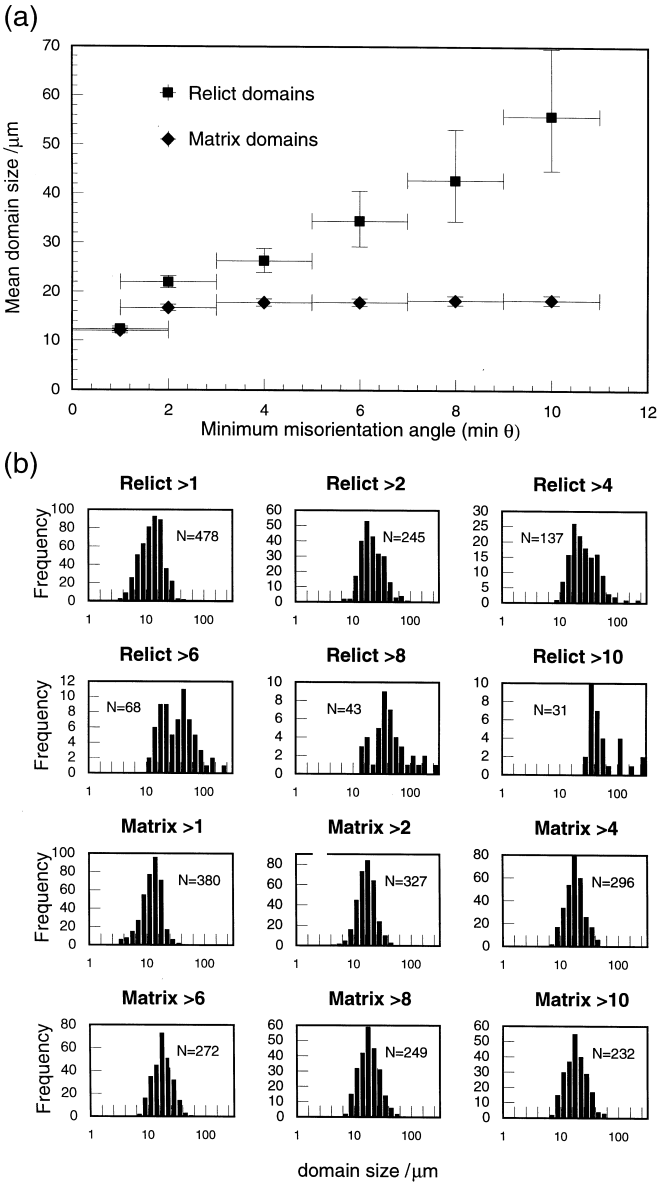

Fig. 6. (a) Mean domain size ($\bar{d}$) plotted against minimum misorientation angle (min θ) showing the grain boundary hierarchy characteristics for the relict grains and the matrix in the low strain zone. Error bars indicate 95% confidence levels. The min $\theta = 1°$ points represent all the observable boundaries in each area. (b) Individual domain size data sets for each misorientation map showing the frequency against log domain size.

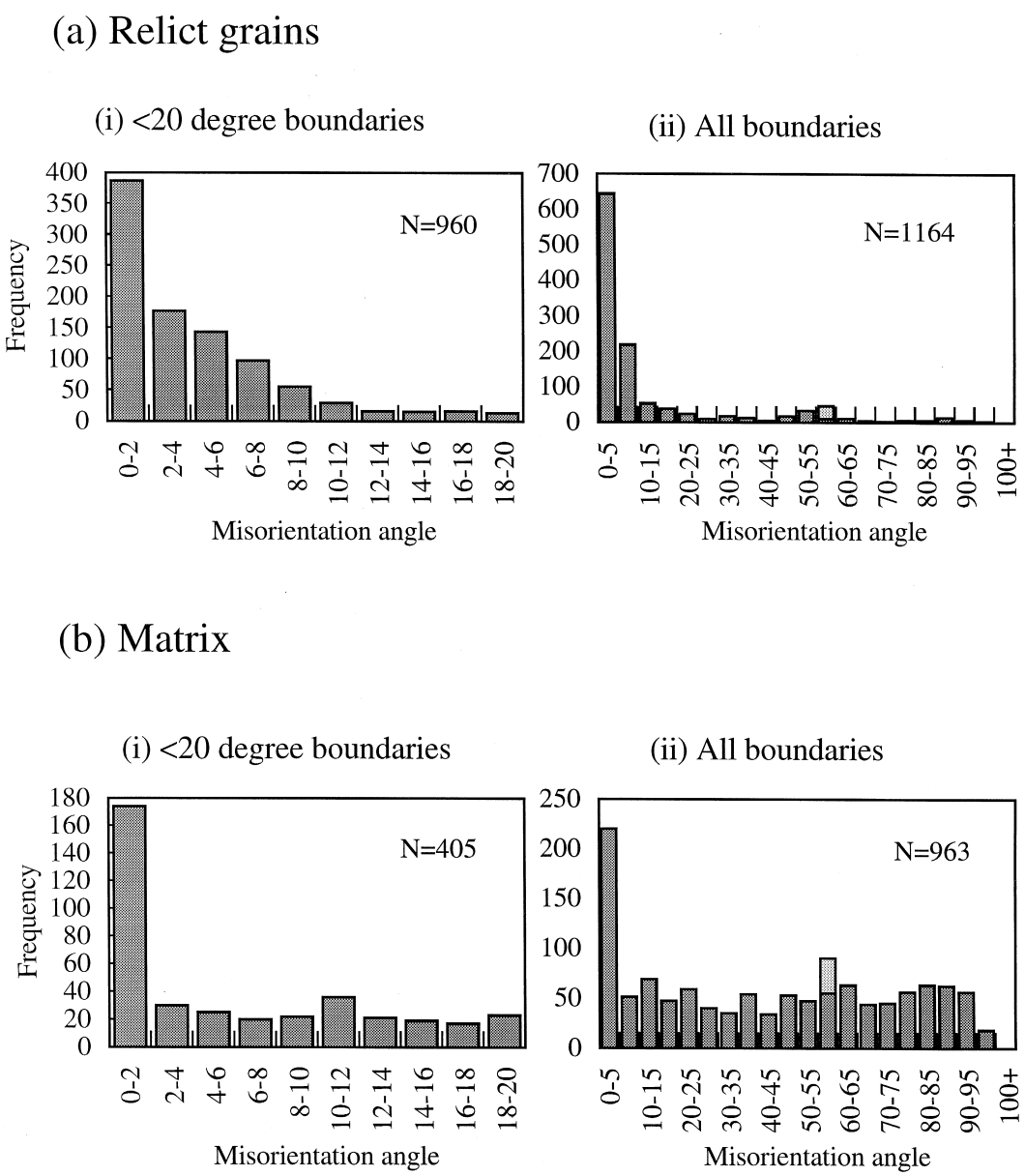

Fig. 7. Boundary misorientation distribution in the low strain zone. (a) The relict grains with (i) boundaries $<20^\circ$ and (ii) all boundaries. Light shading indicates Dauphiné twin boundaries. (b) The matrix with (i) boundaries $<20^\circ$ and (ii) all boundaries. Light shading indicates Dauphiné twin boundaries.

mum at a high angle to the foliation. The *a*-axes define a maximum at an angle of approximately 25° to the lineation direction; thus the *m*-axes will define a maximum almost parallel to the lineation. These data are subtly different to those obtained from a comparable sample discussed in Law *et al.* (1990) but are consistent with dextral shearing (Schmid and Casey, 1986).

Domain boundary hierarchy. Seven hundred and forty nine domains were analysed and the misorientations across 1844 domain boundaries were calculated. Boundary misorientation maps were produced for $\geq 1^\circ$, $\geq 2^\circ$, $\geq 4^\circ$, $\geq 6^\circ$, $\geq 8^\circ$, $\geq 10^\circ$ and $\geq 15^\circ$ boundary misorientations and from these the defined domain sizes were measured. Figure 10 shows two of these misorientation maps, for $\geq 4^\circ$ and $\geq 10^\circ$ misorientations. Clearly there are no larger scale microstructural features as observed in the low strain margin zone. The domain size data are plotted in Fig. 11. For each misorientation map, the domain size distribution is approximately log-normal.

The boundary hierarchy characteristics are close to those of the matrix in the low strain zone, with a distinct step between min $\theta = 1^\circ$ and min $\theta = 2^\circ$ where the domain size jumps from $\bar{d} = 12\ \mu$m to $\bar{d} = 14\ \mu$m, although there are also steps between min $\theta = 2^\circ$ and min $\theta = 4^\circ$ (from $\bar{d} = 14\ \mu$m to $\bar{d} = 16.5\ \mu$m) and between min $\theta = 8^\circ$ and min $\theta = 10^\circ$ (from $\bar{d} = 17\ \mu$m to $\bar{d} = 19\ \mu$m).

Figure 12(a) shows the correlated misorientation distribution frequency for the high strain zone boundaries. As for the low strain zone, there are peaks at $\theta < 5^\circ$ due to the amount of low-angle boundaries and

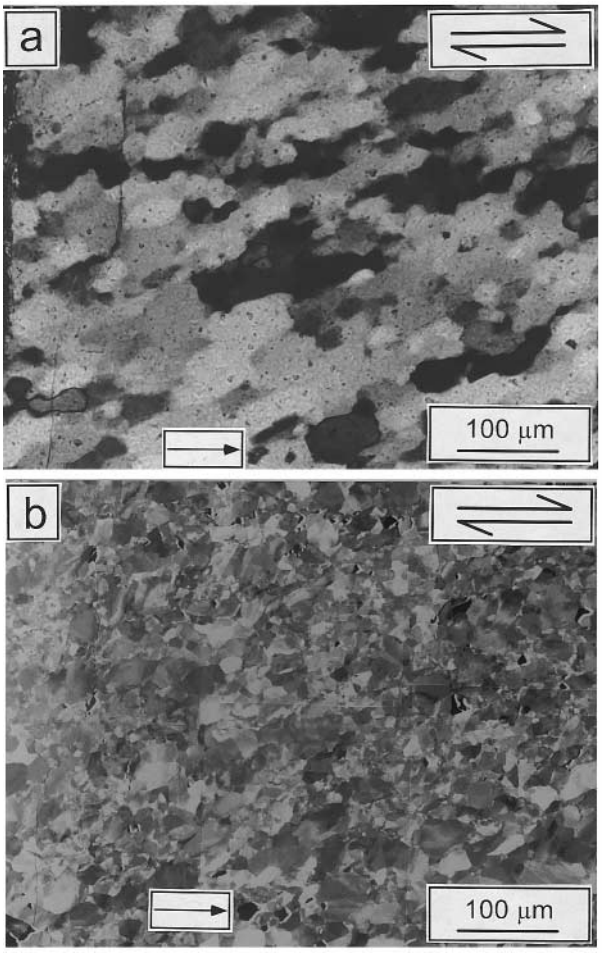

Fig. 8. The high strain interior zone. (a) Photomicrograph taken under crossed polarized light. (b) Forescatter image of the same area taken using the SEM. Operating conditions: Acc.V. 20 kV; WD 27.2 mm. Arrow indicates a polishing blemish visible in both images.

at θ = 55–60° due to a contribution from Dauphiné twinned boundaries (35% of all the boundaries in this misorientation range have rotation axes within 15° of the *c*-axis). However, there are considerably fewer boundaries with misorientations between 5° and 20°. This is clearly illustrated in Fig. 12(b), which shows the misorientation distribution of the lower angle (< 20°) boundaries in this zone. It is also noticeable that there are approximately equal amounts of 0–2° and 2–4° misorientations here, unlike the matrix in the low strain zone.

DISCUSSION

Processes affecting microstructure development

It has already been shown that this shear zone shows the mylonitic foliation orientations expected by simple shearing processes. The change in microstructures from the low strain margin to the high strain interior can be interpreted as a temporal section with increasing strain, but only if it is assumed that the shear zone did not widen with time (Means, 1995). We make this assumption here, although it is hard to justify unequivocally.

To start with we shall consider processes affecting the microstructure development and how they affect the boundary hierarchy characteristics using a qualitative model. Initially we assume that the microstructure consisted of large optical grains defined by boundaries with large misorientations (i.e. > 10°); this has a $\bar{d}$ vs min θ graph with a single horizontal line at a high mean domain size. For simplicity we shall model the hierarchy changes with respect to a one dimensional microstructure as in Fig. 13, using domain length instead of diameter. The basic effects of each microstructural process will remain unchanged. The microstructural and boundary hierarchy characteristics of the protolith are shown in Fig. 13(a). This model is intended to be an aid to understanding the effect of individual processes on the boundary hierarchy and the misorientation distribution, not as an explanation for the development of this shear zone.

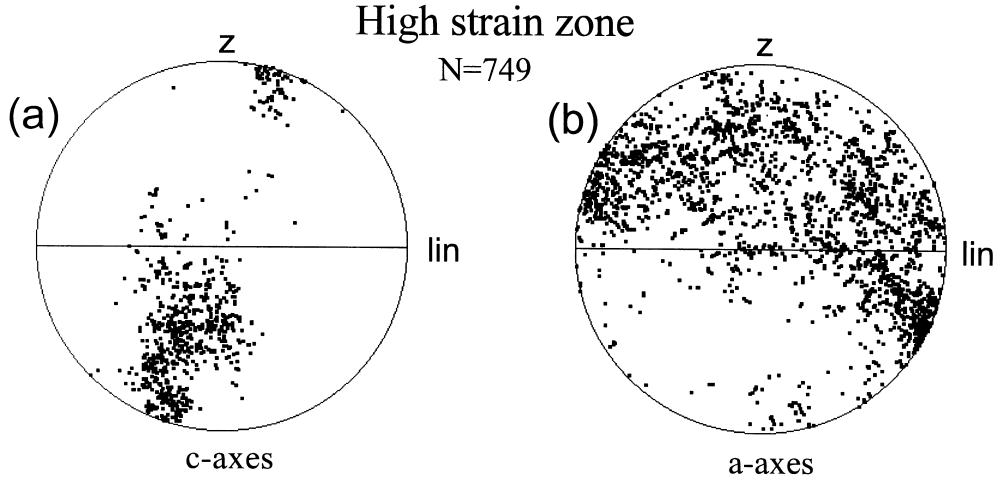

Fig. 9. Pole figures from the high strain zone. (a) *c*-axes. (b) *a*-axes.

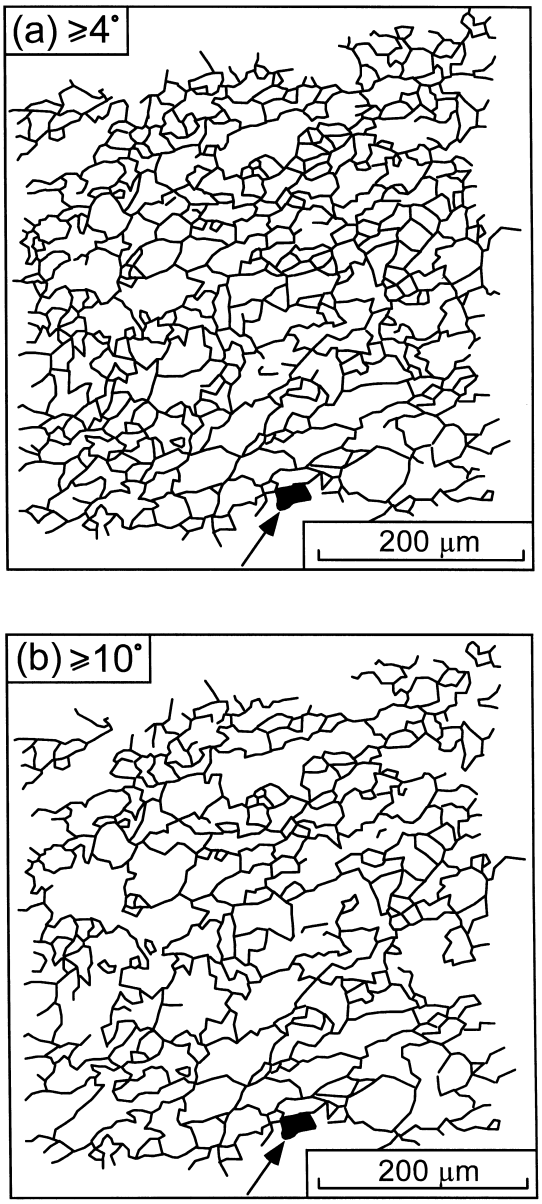

Fig. 10. Boundary misorientation maps for the high strain zone. (a) Boundaries with ≥4° misorientation. (b) Boundaries with ≥10° misorientation. Arrow marks the position of the blemish visible in Fig. 8.

Recovery. Recovery is the process by which subgrain walls are formed, as indicated in the introduction. It is not clear what the mismatch is across a subgrain wall when it is first formed but it is certainly less than 2°. Therefore the process of recovery will decrease the domain size for the min $\theta < 2°$ fraction only, introducing a step into the hierarchy (Fig. 13b). Recovery will also increase the frequency of low angle boundaries in the boundary misorientation distribution.

Subgrain rotation. The continued movement of dislocations of a like sign into an existing subgrain wall has the effect of increasing the misorientation between the two neighbouring crystal lattices. But subgrain rotation may not always increase the misorientations across boundaries; it may be a geometrical necessity that some misorientations decrease. However, the overall effect of subgrain rotation is likely to increase the θ values as shown on the $\bar{d}$ vs min θ and f vs θ graphs (Fig. 13c). If we consider the effect on a discrete hierarchy (as in Fig. 13b), then subgrain rotation will simply increase the θ value at which the domain size step occurs (Fig. 13c). Subgrain rotation will cause a continuous hierarchy (as in Fig. 13d) to maintain its characteristics, but the min θ value for all domain sizes will increase (Fig. 13e). In both cases there will be an increase in the frequency of intermediate angle boundaries (5–15° in the models shown) and a decrease in the frequency of low angle boundaries ($< 5°$ in the models shown).

Subgrain rotation and recovery. The process of recovery combined with subgrain rotation can be modelled fairly simply. If an initially recovered structure with a stepped boundary hierarchy (Fig. 13b) is allowed to undergo subgrain rotation both the smaller and the larger domain sizes will move to higher misorientation values. If a further recovery phase is then allowed, a smaller domain size will be formed for the $\theta = 1°$ fraction. If these processes continue to operate then a continuous boundary hierarchy will develop (Fig. 13d).

Grain boundary migration. The effect of grain boundary migration is to preferentially enlarge some grains at the expense of others. In the absence of nucleation, grain boundary migration alone cannot decrease the average grain size. Lloyd and Freeman (1994) proposed that there is a threshold misorientation θ at which boundary migration may occur at a given temperature. The value of θ is inversely proportional to temperature, consistent with the observations of Hirth and Tullis (1992). Although the existence of a threshold misorientation limits the boundaries which can migrate, all domain types will be affected in the same way: some will be preferentially enlarged at the expense of others causing a general increase in the mean domain size. Figure 13(f) illustrates the possible effect of grain boundary migration on a continuous hierarchy such as that shown in Fig. 13(d).

Continuation of grain boundary migration at a fixed strain rate and temperature is unlikely to lead to a steady increase in grain size. In order for boundary migration to continue there needs to be a driving force, most likely in the form of strain induced defect density variations. This can only occur by the ongoing straining of the crystal lattice so that the boundary hierarchy is then modified by recovery and subgrain rotation or by the nucleation of new grains. Small, new grains would clearly reduce the mean domain size; if these new grains were bounded by medium angle boundaries (perhaps 10–12°, as would be expected with the subgrain bridging nucleation described in Urai *et al.*, 1986) then a step at this min θ value may be produced on the min θ vs $\bar{d}$ graph (Fig. 13g). It is clear that the detailed balance of grain growth and nucleation is hard to predict.

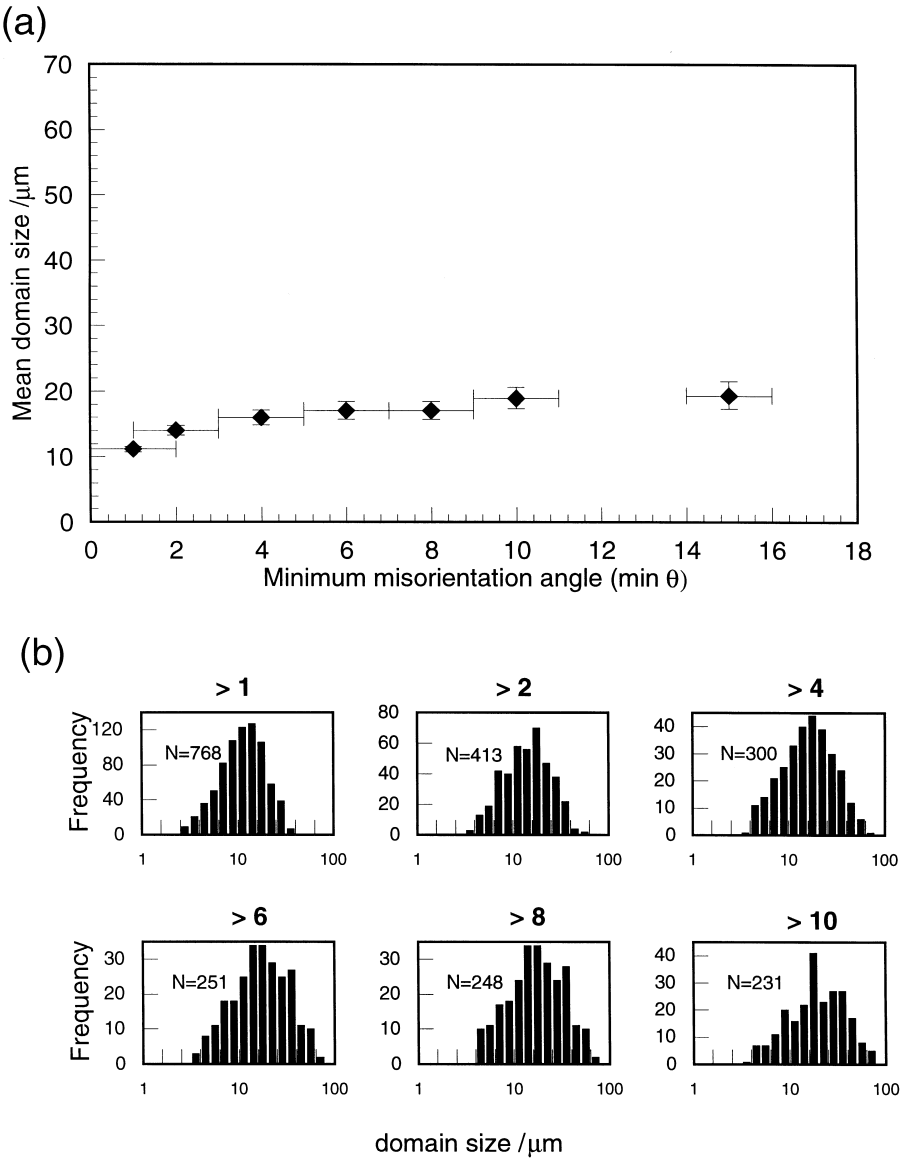

Fig. 11. (a) Mean domain size ($\bar{d}$) plotted against minimum misorientation angle (min θ) for the high strain zone (at the same scale as Fig. 6a). Error bars indicate 95% confidence levels. The min $\theta = 1^\circ$ points represent all the observable boundaries in this area. (b) Individual domain size data sets for each misorientation map showing frequency against log domain size.

The single process of grain boundary migration may also involve some component of grain rotation; it was noted earlier that Cottrell (1964) identified the likelihood of dislocations of one sign to dominate. As the migrating boundary sweeps through the strained lattice, these dislocations will be taken up in the boundary possibly causing a progressive misorientation change to occur. Whether this change will be an increase or a decrease depends purely on the dislocation sign, so it is impossible to predict the effect on the boundary hierarchy characteristics.

Grain boundary sliding. The effect of grain boundary sliding on the boundary hierarchy characteristics is hard to establish. Although there may be scenarios where grain boundary sliding has an identifiable effect on the hierarchy characteristics, the exact nature of these effects is impossible to judge. Thus we shall not consider the effects of grain boundary sliding in this study.

Evidence for the operation of discrete recovery and recrystallization processes

In the relict grains the microstructure is characterized by evenly spaced, straight, low-angle domain boundaries characteristic of the operation of recovery. The boundary misorientation distribution in the relict grains (Fig. 7a) shows the abundance of very low angle ($<2^\circ$) boundaries formed by recovery, but also illustrates the presence of significant number of boundaries with misorientations in the range from 2° to 10°. These are interpreted as being formed by the rotation of the existing subgrain walls. The lack of higher angle boundaries and the preservation of a typical core and

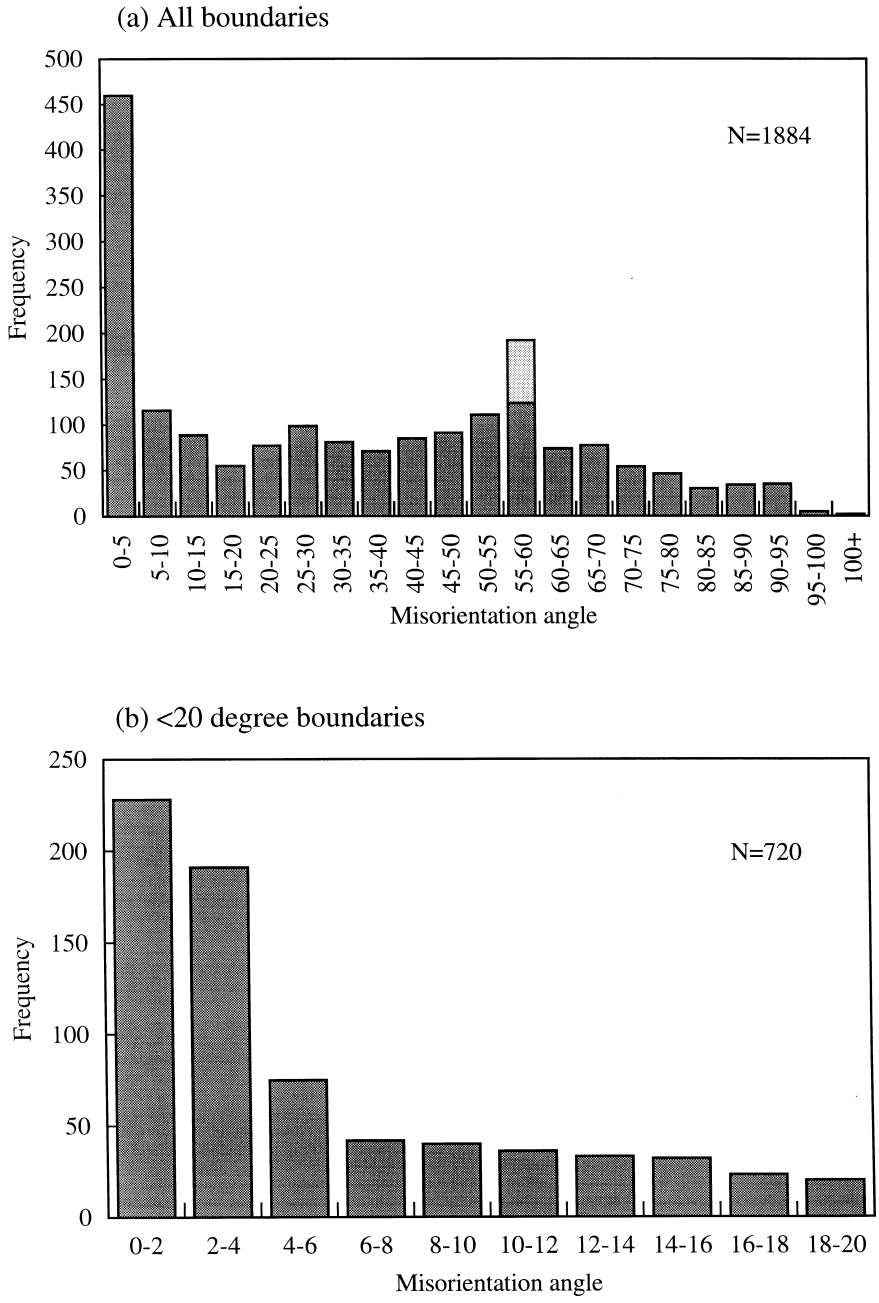

Fig. 12. Boundary misorientation distribution in the high strain zone. (a) All the boundaries. Light shading indicates Dauphiné twin boundaries. (b) Boundaries with misorientations $< 20°$.

mantle microstructure eliminates the possibility of either grain boundary sliding or grain boundary migration within the relict grains.

In the microstructure of the recrystallized quartz outside the relict grains, both in the low and high strain zones, the polygonized signature of a recovery dominated process is not observed. However, there is still an abundance of low-angle boundaries and considerable subgrain microstructure can be observed within the optical grains, suggesting that recovery is a process which is operating throughout the development of these microstructures.

Figure 14 illustrates the approach taken in a number of studies of boundary misorientation characteristics (e.g. Fliervoet and White, 1995; Lloyd and Freeman, 1991, 1994; Lloyd *et al.*, 1997). For each of the typical microstructures, we have considered the boundaries in a traverse, using the rotation axes as well as the angular misorientation. The results suggest that a significant proportion of the boundary misorientations can be described in terms of simple tilt boundaries, involving rotation about a single crystallographic axis. In the transect across a relict grain (Fig. 14a), 66% of the boundaries can be attributed to the operation of a single slip system (e.g. basal-*m* slip about *a* axes). In the low strain matrix (Fig. 14b) 55% are due to single slip systems, whilst in the high strain interior this decreases to only 33% (Fig. 14c). This confirms the

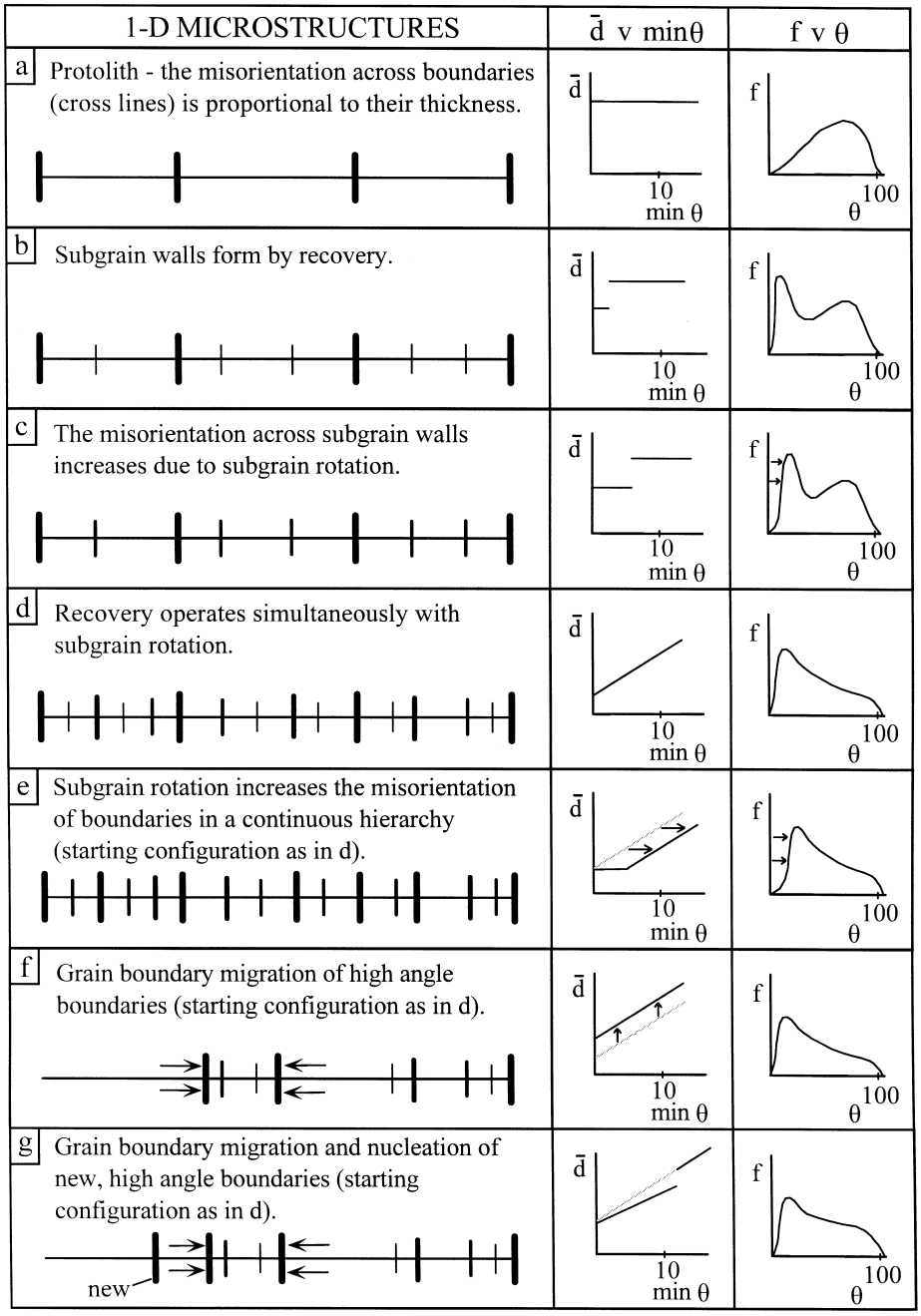

Fig. 13. Schematic one-dimensional model illustrating the effects of individual processes on the microstructure and the boundary hierarchy characteristics. (a) The protolith. (b) Recovery. (c) Subgrain rotation. (d) Recovery combined with subgrain rotation. (e) Subgrain rotation operating on a continuous hierarchy. (f) Grain boundary migration operating on a continuous hierarchy. (g) Grain boundary migration combined with nucleation.

conclusion that the low angle boundaries within the relict grains are formed by simple tilting events, whilst other processes such as grain boundary migration become more important in the other microstructural zones. However, some caution must be exercised when using this approach: the angular error in determining the rotation axis can become significant when looking at very low angle boundaries.

As mentioned earlier, the operation of grain boundary migration is characterized by the presence of sutured grain boundaries in optical microscopy. Sutured boundaries can clearly be seen in the high strain zone in Fig. 8(a), whilst less clear evidence is visible in the low strain matrix in Fig. 3(a). Clearly grain boundary migration was an important process in the high strain zone and was also operating, to a lesser extent, in the low strain matrix.

Explanation of the observed hierarchies

The continuous hierarchy in the relict grains (Fig. 6a) can easily be explained by the combined op-

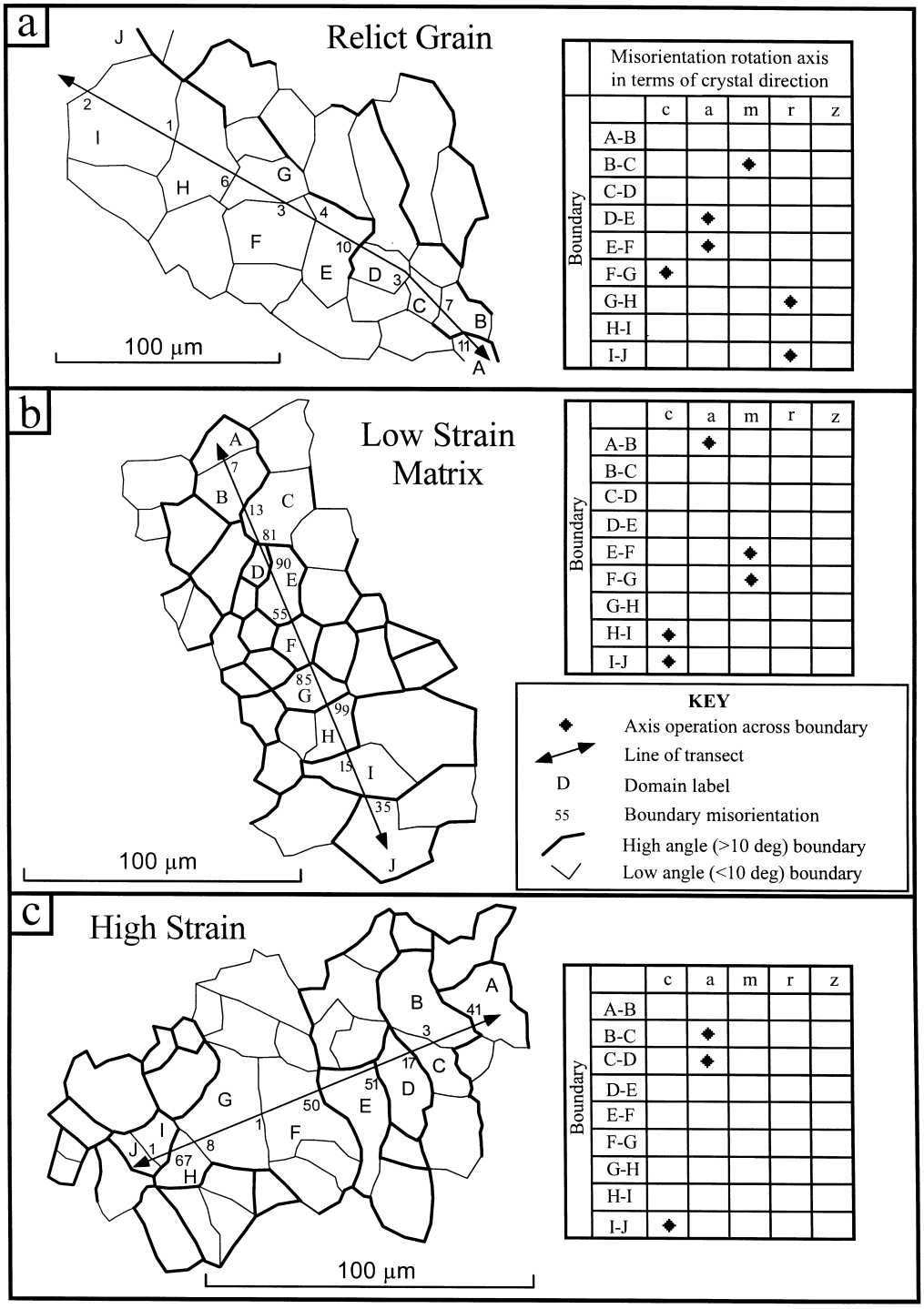

Fig. 14. Details of transects across each of the microstructural zones. Coincidence relationships across each domain boundary are shown (where identified), indicating the operation of specific slip systems. (a) Low strain relict grain. (b) Low strain matrix region. (c) High strain region.

eration of recovery and subgrain rotation as described earlier. However, the process of evolving this hierarchy into the stepped hierarchy of the matrix is more complex. The low angle ($\theta = 1°$) domain size stays approximately constant, whilst the higher angle domain size effectively decreases. In order to produce the horizontal line between $\theta = 2°$ and $\theta = 10°$ in the min θ vs $\bar{d}$ graph, all the boundaries with misorientations in this range must either be eliminated or have their misorientations altered. The effect of subgrain rotation on the boundaries within this range could increase their misorientations to $>10°$, thus producing the horizontal line in the min θ vs $\bar{d}$ graph. However, it would be likely that subgrain rotation would also increase the misorientation of the very low angle ($<2°$) subgrain walls, moving the step in the min θ vs $\bar{d}$ graph to a

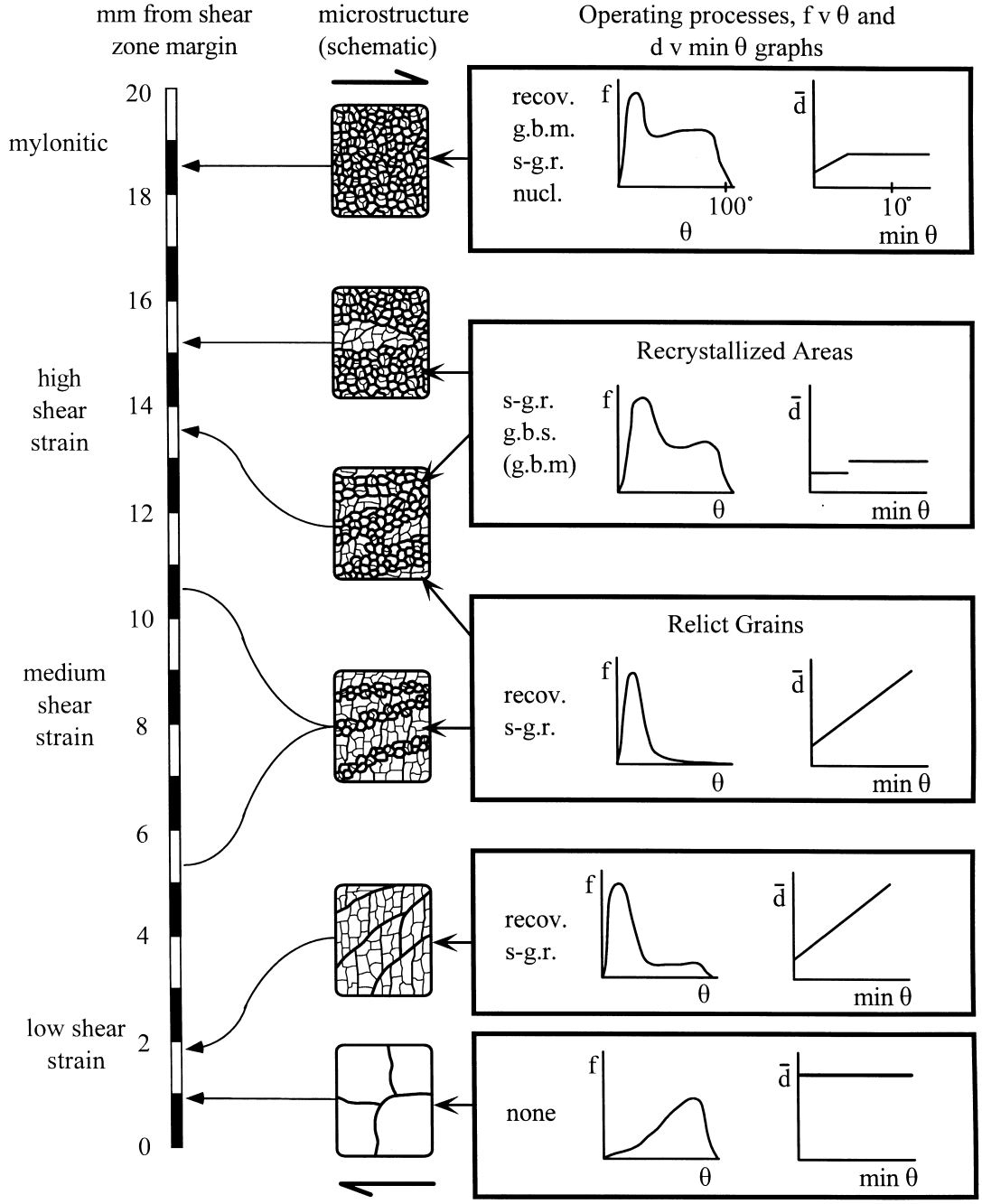

Fig. 15. Summary diagram showing the possible microstructural development along a shear zone margin to interior transect. Expected/observed f–θ and $\bar{d}$–min θ characteristics are shown. See text for discussion.

higher min θ value. This step stays at the same place, so subgrain rotation alone cannot explain this hierarchy.

The boundary hierarchies of the low strain matrix and the high strain zone are essentially the same: there is a distinct increase in domain size at min $\theta \approx 2^\circ$ and the domain size for min $\theta > 4^\circ$ is approximately constant (18–19 μm). However, there are some subtle but significant changes. Although the domain size defined by the very low angle boundaries stays the same ($\approx$12 μm), the step in domain size that exists between min $\theta = 1^\circ$ and min $\theta = 2^\circ$ is replaced by a more continuous increase from min $\theta = 1^\circ$ to min $\theta = 6^\circ$ in the high strain zone and the domain size defined by the higher angle ($\geq 10^\circ$) boundaries increases from 17 μm to 19 μm. These changes cannot be explained by the operation of a single process. However, a combination of grain boundary migration (increases all domain sizes), recovery combined with subgrain rotation (decreases the lower angle domain sizes and produces the continuous rise up to min $\theta = 6^\circ$) and the nucleation of new grains (prevents a large increase in higher

angle domain size) could explain the change. It is difficult to establish the relative importance of each of the processes in altering the boundary hierarchy characteristics, but it seems likely that some cyclic process involving all of them is operating.

Microstructural evolution of the shear zone

Combining the microstructural and boundary hierarchy data with a margin to interior transect allows us to suggest a microstructural evolution path for this shear zone. Figure 15 is a summary of the data in such a margin to interior transect. The protolith microstructure is initially altered by the combined processes of recovery and subgrain rotation. As these relict grains bend around into the mylonitic foliation, high strain gradients are formed in the boundary regions and it is here that recrystallization by continued rotation and grain boundary sliding occurs. The partitioning of strain into these boundary zones causes the microstructure within the relict grains to be 'frozen' until much higher strains are attained. This initially forms a core and mantle microstructure, but wider bands of recrystallized matrix soon develop. With increasing strain and, possibly, strain rate, grain boundary migration becomes a more important process and the relict grains become completely recrystallized. A cyclic balance between recovery, subgrain rotation, grain boundary migration and nucleation may have been attained, which would give a steady state microstructure. However, individual elements continued to evolve, allowing the continuation of strain accommodation and deformation.

The orientation of the relict grains may still have an effect on the orientation of the recrystallized grains since, with no dominant grain boundary sliding processes likely, the main mechanisms of recrystallization ensure that new grains have their orientations controlled by the original grains. For instance, the formation of new grains from the original relict grain by subgrain rotation means that the new grains are linked to the original orientation by some simple slip system: if this is a basal prism slip system about the *c*-axis then the new grains will share the same *c*-axis orientations as their predecessor. New grains formed by grain boundary migration are related to adjacent grains. However, the adjacent grains are likely to have been derived from the same original (relict) grain; therefore the new grains may also possess crystallographic similarities to the original relict grain. This may help to explain the occurrence of elongate domains in the high strain interior with similar crystallographic orientations, although some authors have suggested that other mechanisms are responsible for the formation of these domains (e.g. Knipe and Law, 1987; Lloyd *et al.*, 1992).

Implications for palaeopiezometry

The use of recrystallized grain sizes and subgrain sizes of quartz in quartzose mylonitic rocks to determine palaeostress estimates is common (e.g. Ord and Christie, 1984; Prior *et al.*, 1990; Michibayashi, 1993). A number of palaeopiezometers have been calculated, both empirically and theoretically (e.g. Twiss, 1977, 1986; Edward *et al.*, 1982), but these still give a wide range of stress estimates. For all these piezometers it is necessary to assume that the microstructure is in a steady state condition. If the discrete hierarchies seen in the recrystallized bands and, to an extent, in the high strain interior are representative of steady state deformation, then grain boundary hierarchies could be a reliable method of assessing the suitability of any microstructure for palaeopiezometric work. Furthermore, they could be used to identify when a subgrain size does relate to the overall stress field. The existing subgrain palaeopiezometers give a range of stress estimates from 7 MPa (Twiss, 1977) to 35 MPa (Twiss, 1986) for a subgrain size of 12 μm. A corresponding grain size of 19 μm produces stress estimates ranging from 18 MPa (White, 1979) to 100 MPa (Twiss, 1977). It may be possible to calibrate empirically a palaeopiezometer using boundary hierarchy data, defining the stress corresponding to the domain sizes defined by different misorientation values. Presently there is no palaeopiezometer which gives the same stress estimate from both the grain and subgrain size measurements.

It is also clear that the continuous hierarchy of subgrains in the relict grains cannot be used for palaeopiezometry: firstly the hierarchy indicates that the recrystallization processes needed in a steady state cycle were never properly reached and secondly, when using a subgrain size, what misorientation value should be taken? Each minimum θ defines a different subgrain size. Further investigation into the consequence of boundary hierarchies with respect to palaeopiezometers is necessary.

SUMMARY AND CONCLUSIONS

1. Optical and forescatter imaging combined with EBSD work has identified the nature of any boundary hierarchy in the low strain margin and high strain interior of a sheared quartz vein.

2. The relict grains in the low strain margin show a continuous boundary hierarchy whilst the recrystallized areas generally show a discrete boundary hierarchy.

3. The hierarchy characteristics can be related to the recrystallization processes. Recovery combined with subgrain rotation results in the continuous hierarchy observed in the relict grains. The discrete hierarchy of the fine grained matrix around the relict grains and in

the high strain zone cannot be related to recovery and subgrain rotation alone. Instead it indicates a combination of recovery, subgrain rotation, grain boundary sliding, grain boundary migration and nucleation. This conclusion is reinforced by detailed transects incorporating the misorientation rotation axes as well as the angular magnitudes.

4. The microstructural evolution of a simple shear zone such as this can be deduced from a combination of the microstructure, the crystallographic fabric and the boundary hierarchy characteristics.

5. A discrete hierarchy may indicate a steady state microstructure: this could have implications for the use of grain and subgrain size palaeopiezometers, and it may help with a more accurate empirical recalibration.

6. Similar boundary hierarchy investigations are required on other specimens where the conditions during deformation are better constrained.

7. In order for the technique to be practically useful, an automated method of collecting boundary hierarchy data is necessary. This will probably be with a fully automated beam shift and EBSP collection/recognition system commonly used in material sciences and metallurgy (e.g. Adams *et al.*, 1994; Kunze *et al.*, 1995). However, problems of specimen charging and the automatic recognition of the pseudo-symmetry of quartz diffraction patterns need to be overcome.

Acknowledgements—We would like to thank HKL software (in particular Niels-Henrik Schmidt and Berndt Neumann) for the CHANNEL+ indexing program. Kees Veltkamp is thanked for his SEM expertise and advice. The Liverpool SEM was funded by the University of Liverpool Research Task Force. We are very grateful to Timon Fliervoet for his help with the production of misorientation distribution data and for his comments on an early version of the manuscript. The comments of Graham Potts, the journal's editor, Peter Hudleston, and reviewers, Geoff Lloyd and an anonymous reviewer, contributed significantly to the final version of this paper. P. W. Trimby acknowledges receipt of a UK NERC studentship.

REFERENCES

Adams, B. L., Dingley, D. J., Kunze, K. and Wright, S. I. (1994) Orientation imaging microscopy: new possibilities for microstructural investigations using automated BKD analysis. In *Textures of Materials (Proc. ICOTOM 10)*, ed. H. J. Bunge, pp. 157–162. Materials Science Forum, **31**.

Alam, M. N., Blackman, M. and Pashley, D. W. (1954) High-angle kikuchi patterns. *Proceedings of the Royal Society* **222,** 24–242.

Cottrell, A. H. (1964) *Theory of Crystal Dislocations*. Gordon and Breach, London.

Dingley, D. J. (1984) Diffraction from sub-micron areas using electron backscattering in a scanning electron microscope. *Scanning Electron Microscopy* **1984-II,** 569–575.

Dingley, D. J. and Randle, V. (1992) Microtexture determination by electron back-scatter diffraction. *Journal of Material Science* **27,** 4545–4566.

Drury, M. R. and Urai, J. L. (1990) Deformation-related recrystallisation processes. *Tectonophysics* **172,** 235–253.

Edward, G. H., Etheridge, M. A. and Hobbs, B. E. (1982) On the stress dependence of subgrain size. *Textures and Microstructures* **5,** 127–152.

Fitzgerald, J. D., Etheridge, M. A. and Vernon, R. H. (1983) Dynamic recrystallisation in a naturally deformed albite. *Textures and Microstructures* **5,** 219–237.

Fliervoet, T. F. (1995) Deformation mechanisms in fine grained quartzo-feldspathic mylonites. An electron microscopy study. Ph.D. thesis. Utrecht University, Geologica Ultraiectina, 131 p.

Fliervoet, T. F. and White, S. H. (1995) Quartz deformation in a very fine grained quartzo-feldspathic mylonite: a lack of evidence for dominant grain boundary sliding deformation. *Journal of Structural Geology* **17,** 1095–1109.

Fliervoet, T. F., White, S. H. and Drury, M. R. (1997) Evidence for dominant grain-boundary sliding deformation in greenschist- and amphibolite-grade polymineralic ultramylonites from the Redbank Deformed Zone, Central Australia. *Journal of Structural Geology* **19,** 1495–1520.

Guillopé, M. and Poirier, J. P. (1979) Dynamic recrystallisation during creep of single crystalline halite: an experimental study. *Journal of Geophysical Research* **84,** 5557–5567.

Hirth, G. and Tullis, J. (1992) Dislocation creep regimes in quartz aggregates. *Journal of Structural Geology* **14,** 145–159.

Hobbs, B. E., Means, W. D. and Williams, P. F. (1976) *An Outline of Structural Geology*. John Wiley and Sons, New York.

Knipe, R. J. and Law, R. D. (1987) The influence of crystallographic orientation and grain boundary migration on microstructural and textural evolution in an *S–C* mylonite. *Tectonophysics* **135,** 155–169.

Kunze, K., Heidelbach, F., Wenk, H.-R. and Adams, B. L. (1995) Orientation imaging microscopy of calcite rocks. In *Textures of Geological Materials*, eds H. J. Bunge, S. Siegesmunde, W. Skrotski and K. Weber, pp. 127–144. DGM Informationsgesellschaft MbH.

Law, R. D., Schmid, S. M. and Wheeler, J. (1990) Simple shear deformation and quartz crystallographic fabrics: a possible natural example from the Torridon area of NW Scotland. *Journal of Structural Geology* **12,** 29–45.

Lloyd, G. E. (1987) Atomic number and crystallographic contrast images with the SEM: a review of backscattered electron techniques. *Mineralogical Magazine* **51,** 3–19.

Lloyd, G. E., Ferguson, C. C. and Law, R. D. (1987) Discriminatory petrofabric analysis of quartz rocks using SEM electron channelling. *Tectonophysics* **135,** 243–249.

Lloyd, G. E. and Freeman, B. (1991) SEM electron channelling analysis of dynamic recrystallization in a quartz grain. *Journal of Structural Geology* **13,** 945–953.

Lloyd, G. E., Law, R. D., Mainprice, D. and Wheeler, J. (1992) Microstructural and crystal fabric evolution during shear zone formation. *Journal of Structural Geology* **14,** 1079–1100.

Lloyd, G. E. and Freeman, B. (1994) Dynamic recrystallisation of quartz under greenschist conditions. *Journal of Structural Geology* **16,** 867–881.

Lloyd, G. E. (1995) An appreciation of the SEM electron channelling technique for petrofabric and microstructural analysis of geological materials. In *Textures of Geological Materials*, eds H. J. Bunge, S. Siegesmund, W. Skrotzki and K. Weber, ISBN 3-88355-200-3, pp. 109–125. DGM Informationsgesellschaft MbH.

Lloyd, G. E., Farmer, A. B. and Mainprice, D. (1997) Misorientation analysis and the formation and orientation of subgrain and grain boundaries. *Tectonophysics* **279,** 55–78.

McLaren, A. C. (1986) Some speculations on the nature of high-angle grain boundaries in quartz rocks. In *Mineral and Rock Deformation: Laboratory Studies—The Paterson Volume*, eds B. E. Hobbs and H. C. Heard, pp. 233–245. American Geophysical Union Geophysical Monograph, **36**.

Means, W. D. (1989) Synkinematic microscopy of transparent polycrystals. *Journal of Structural Geology* **11,** 163–174.

Means, W. D. (1995) Shear zones and rock history. *Tectonophysics* **247,** 157–160.

Michibayashi, K. (1993) Syntectonic development of a strain-independent steady state grain size during mylonitization. *Tectonophysics* **222,** 151–164.

Ord, A. and Christie, J. M. (1984) Flow stresses from microstructures in mylonitic quartzites of the Moine Thrust zone, Assynt area, Scotland. *Journal of Structural Geology* **6,** 639–654.

Poirier, J. P. and Nicolas, A. (1975) Deformation induced recrystallisation due to progressive misorientation of subgrains, with special reference to mantle peridotites. *Journal of Geology* **83,** 707–720.

Prior, D. J., Knipe, R. J. and Handy, M. R. (1990) Estimates of the rates of microstructural changes in mylonites. In *Deformation Mechanisms, Rheology and Tectonics*, eds R. J. Knipe and E. H. Rutter, pp. 309–319. Geological Society Special Publication. **54**.

Prior, D. J., Trimby, P. W., Weber, U. D. and Dingley, D. J. (1996) Orientation contrast imaging of microstructures in rocks using forescatter detectors in the scanning electron microscope. *Mineralogical Magazine* **60,** 859–869.

Ramsay, J. G. and Graham, R. H. (1970) Strain variation in shear belts. *Canadian Journal of Science* **7,** 786–813.

Randle, V. and Ralph, B. (1986) A practical approach to the determination of the crystallography of grain boundaries. *Journal of Material Science* **21,** 3823–3828.

Randle, V. (1992) *Microtexture determination and its applications*. The Institute of Materials, London.

Schmid, S. M. and Casey, M. (1986) Complete fabric analysis of some commonly observed quartz *c*-axis patterns. In *Mineral and Rock Deformation: Laboratory Studies—The Paterson Volume*, eds B. E. Hobbs and H. C. Heard, pp. 263–286. American Geophysical Union Geophysical Monograph, **36**.

Schmidt, N.-H. and Olesen, N. O. (1989) Computer-aided determination of crystal lattice orientation from electron channelling patterns in the SEM. *Canadian Mineralogist* **27,** 15–22.

Twiss, R. J. (1977) Theory and applicability of a recrystallised grain-size palaeopiezometer. *Pure and Applied Geophysics* **115,** 227–244.

Twiss, R. J. (1986) Variable sensitivity piezometric equations for dislocation density and subgrain diameter and their relevance to olivine and quartz. In *Mineral and Rock Deformation: Laboratory Studies—The Paterson Volume*, eds B. E. Hobbs and H. C. Heard, pp. 247–263. American Geophysical Union Geophysical Monograph, **36**.

Urai, J. L., Means, W. D. and Lister, G. S. (1986) Dynamic recrystallisation of minerals. In *Mineral and Rock Deformation: Laboratory Studies—The Paterson Volume*, eds B. E. Hobbs and H. C. Heard, pp. 161–199. American Geophysical Union Geophysical Monograph, **36**.

Venables, J. A. and Harland, C. J. (1972) Electron back-scattering patterns—a new technique for obtaining crystallographic information in the scanning electron microscope. *Philosophical Magazine* **27,** 1193–1200.

White, S. H. (1976) The effects of strain on the microstructures, fabrics and deformation mechanisms in quartz. *Philosophical Transactions of the Royal Society of London* **A283,** 69–86.

White, S. H. (1979) Grain and sub-grain size variations across a mylonite zone. *Contributions to Mineralogy and Petrology* **70,** 193–202.

White, S. H. (1977) Geological significance of recovery and recrystallisation processes in quartz. *Tectonophysics* **39,** 143–170.

White, S. H., Burrows, S. E., Carreras, J., Shaw, N. D. and Humphreys, F. J. (1980) On mylonites in ductile shear zones. *Journal of Structural Geology* **2,** 175–187.

White, J. C. and White, S. H. (1981) On the structures of grain boundaries in tectonites. *Tectonophysics* **78,** 613–628.